RSC Advances

ROYAL SOCIETY OF CHEMISTRY

www.rsc.org/advances

Facile identification of the critical content of multi-layer graphene oxide for epoxy composite with the optimal thermal properties

Tianle Zhou[a,*], Shijo Nagao[b], Tohru Sugahara[b], Hirotaka Koga[b], Masaya Nogi[b], Katsuaki Suganuma[b], Thi Thi Nge[c], Yuta Nishina[d]

[a]School of Materials Science and Engineering, Nanjing University of Science and Technology, Nanjing 210094, China

[b]The Institute of Scientific and Industrial Research, Osaka University, Mihogaoka 8-1, Ibaraki, Osaka 567-0047, Japan

[c]Wood Chemistry Laboratory, Department of Biomass Chemistry, Forestry and Forest Products Research Institute, 1 Matsunosato, Tsukuba, Ibaraki 305-8687, Japan

[d]Research Core for Interdisciplinary Science, Okayama University, Tsushimanaka, Kita-ku, Okayama 700-8530, Japan

Abstract- Multi-layer graphene oxide (MGO) has attracted considerable interest in conductive polymer composites. However, in most cases the optimal MGO content is determined by using complex procedure. Without the most complicated works in processing polymerized samples followed by testing various properties, here, a facile strategy is proposed to directly identify the critical MGO content among formulations for epoxy composite with the optimal thermal properties, simply by monitoring the "unusual" nonlinear MGO content-dependent cure behaviors as well as the "unusual" pattern of double-peak of curing curves. The formation mechanism of the double-peak pattern was explored with an emphasis given to the study of epoxy-MGO reaction by using modified Shrinking Core Model. The optimal content determined in this work

*Corresponding author. TEL: +86-025-52748295, E-mail: ztltianle999@hotmail.com (Tianle Zhou)

(2wt% MGO) was verified by the thermal properties (thermal conductivity, structural thermal stability and coefficient of thermal expansion) of MGO/epoxy composites. Based on the inherent relationship between the effect of MGO percolating chains on the thermal polymerization behavior and the resulting thermal properties, this strategy can be easily extended to different kinds of conductive MGO/polymer composites.

1. Introduction

Unprecedented endeavor in exploiting graphene oxide (GO), due to its fascinating and especially technologically useful properties [1-4], calls for methods to efficiently determine the optimal usage amount of GO for the benefits of diversified applications and academic researches for potential applications, particularly in the case of conductive polymer composites which play vital roles for the long life and high performance of electronic and photonic devices in advanced systems such as printed electronics[5-8].

Apart from the guidance of numerical methods (molecular dynamics simulation [9]; statistical, thermodynamic and structure-oriented percolation models [10, 11], etc), so far, the most widely applied procedure in determining the optimal GO content for polymer composites involves [12-15]: (a) preparing composite mixtures with different GO content, (b) polymerizing, (c) processing polymerized samples (cutting, grinding, finely polishing, etc), (d) testing various properties, and finally (e) identifying the critical GO content among formulations for polymer composites with the optimal properties. This procedure, especially steps (c, d), is complicated and time-consuming, severely hindering the rapid development of GO/polymer composites.

It is worth noting that step (b) plays an important role in determining the final properties of GO/polymer composites. Great efforts have been stimulated to describe the influences of GO on the polymerization processes, e.g. those of benzoxazine [16],

ethylene-propylene-diene rubber [17], cyanate ester resin [18], poly(L-lactic acid) [19], tetrafunctional tetraglycidyl-4,4'-diaminodiphenylmethane [20], epoxy/amine [21], epoxy/anhydride [22], poly(3-hydroxybutyrate) [23, 24], photocured epoxy [25, 26] and poly(3,4-ethylenedioxythiophene)-*block*-poly (ethylene glycol)/polyvinylidenefluoride [27]. As a result, the influence mechanisms of GO on the structural [16-18, 23-25], thermal [16, 20, 22, 23, 27], dielectric [25] and mechanical [22, 25, 26] properties of GO/polymer composites were clarified, optimized polymerization strategies were accordingly further proposed for obtaining composites with higher performance [18, 25, 26], but no strategy for determining the optimal GO content has been developed yet.

To address this problem, here, for the first time, we propose an effective strategy to directly identify the critical multi-layer GO (MGO) content for epoxy composite with the optimal thermal properties by monitoring "unusual" effects of MGO on the thermal curing process of epoxy. Based on a solid basis i.e. the inherent relationship between the effect of MGO percolating chains on the thermal polymerization behavior and the resulting thermal properties, this strategy has a great potential for widespread use in conductive MGO/polymer composites.

2. Experimental

2.1 Materials

So far, GO has been extensively utilized in polymer composites. Besides the lower cost and higher yield production than graphene, GO is heavily oxygenated (its basal plane carbon atoms are decorated with -OH and C-O-C groups, while -OH and -COOH groups at the edge), not only enabling an improved GO/polymer interfacial interaction, but also facilitating better dispersion state of GO in matrix [1, 2]. Since monolayer or few-layer GO not necessarily gives the best reinforcement because too much amount of

wrinkling of GO weakens its effectiveness for forming conductive network, therefore, MGO is more desirable in this work. MGO/water mixture (Rap GO TQ2, low oxidation grade) was supplied by NiSiNa materials Co., Ltd, Japan. Before being used, MGO/water mixture was moderately centrifugated (10000 rpm, 10min) with abundant ethanol for 3 times to replace water solvent with ethanol solvent as well as removing any agglomerated MGO sheets.

Diglycidyl ether of bisphenol-A (DGEBA)/2-ethyl-4-methylimidazole (EMI-2,4) system, a widely used epoxy system in industries, was employed herein. Epon 828, supplied by Shanghai Resin Co. Ltd., China, is basically DGEBA with epoxy value of 0.48-0.52mol/100g. Curing agent EMI-2,4 was supplied by Wako Pure Chemical Industries, Ltd., Japan. The employed weight ratio of DGEBA and EMI-2,4 was 100:6. Graphite particles (sized at ~500μm, carbon content >99%) were supplied by Xinfangyuan Co. Ltd., China. Other agents utilized were analytically pure grade and supplied by Wako Pure Chemical Industries, Ltd., Japan.

2.2 Preparation of MGO/DGEBA/EMI-2,4 composite mixture

A certain amount of MGO/ethanol mixture was mixed with DGEBA and EMI-2,4 (MGO/ethanol mixture was sonicated for 1.5h in advance to break down MGO agglomerates), then the mixture was stirred with a rotation speed of 2000 rpm as well as a simultaneous revolution speed of 2000 rpm for 6 times (each time for 5 min) by using Thinky Mixer (ARV310, Thinky Co. Japan), a vacuum pressure reduction function of which removed volatile solvents and submicron trapped air bubbles as well as giving an outstanding dispersion performance (This step is unique in comparison with other methods for nanocarbon-based composite preparation, not only because most of the ethanol solvent can be removed during the mixing process, but also because excellent

dispersion of nanocarbon fillers is guaranteed as the solvent reduces). Each time after mixing for 5min, an ice bath was used to keep the temperature of the mixture around 283K (low-temperature treatment produces better nanofiller dispersion state than high temperature [28] as well as preventing from an untimely occurrence of curing), then the mixture was weighted to determine the precise amount of MGO introduced into matrix and the amount of MGO/water mixture needed to add. Repeating this process until the MGO content was 0.5, 1, 2 or 3% by weight of epoxy resin.

2.3 Preparation of MGO/epoxy composite

MGO/epoxy composite was prepared by in-situ polymerization. Although Thinky Mixer uses sophisticated approaches in removing solvents during mixing and thus reducing the defects of voids and pores in the final composite, it is necessary to degass the mixture after the casting step to remove the air absorbed during this step. The basic preparation process involved (a) casting mixture in mould, (b) repeatedly degassing the mixture in vacuum drying oven at 313K until no air bubble appears on the surface of the mixture, (c) curing the mixture at 313K for 1h, 378K for 1.5h, and 458K for 1.5h, and (d) cooling to room temperature, then demoulding.

2.4 Characterization

Morphological studies were carried out using transmission electron microscopy (TEM, JEM-3000F, JEOL Japan Co., Ltd. and FEI TECNAI G2 20, FEI Co., Ltd.) and field emission scanning electron microscopy (FE-SEM, JSM-6700F, JEOL Japan Co., Ltd.). For the TEM observation, the diluted MGO dispersion was dropped onto a carbon coated copper grid and allowed to dry under ambient conditions. As for the composites, an ultrathin section of the specimen with a thickness of 80nm was prepared using an ultramicrotome (Leica UC6, Leica Co., Ltd.) with a diamond knife. Specimens were

coated with a thin platinum layer before FE-SEM observation.

Infrared spectra were tested using FT-IR spectrometer (Perkin-Elmer frontier, Perkin-Elmer Japan Co., Ltd.) for evaluating the functional groups of MGO, the hydrogen bonds at MGO/epoxy interface as well as the whole epoxy curing degree (α_{IR}). The spectra were obtained by averaging 16 scans in a range of frequency from 4000 to 700 cm^{-1} with a resolution of 4 cm^{-1} followed by subtracting the background curve. Attenuated total reflectance spectra were collected from the polymeric films. α_{IR} was obtained by measuring the reactive absorbance of epoxy band (914 cm^{-1}) against the absorbance of the band of benzene ring (1610 cm^{-1}) which acts as a reference. These absorbances were calculated in the spectra processed by a base-line correction to obtain comparable results. A set of three specimens was tested for each material after pre-dried in air at 373K for 12h.

Approximately 4 mg MGO/DGEBA/EMI-2,4 mixture was weighed accurately into an aluminum differential scanning calorimetry (DSC) sample pan and then covered with an aluminum lid. DSC measurements were carried out by using a NETZSCH DSC 204 F1 system (NETZSCH Instruments Japan Co., Ltd.). The DSC was calibrated with high purity indium; a-Al_2O_3 was used as the reference material. Dynamic experiments were carried out under an argon flow rate of 25 ml/min and a temperature ranging from 313 to 623K at different heating rates of 10, 15, 20, 25 K/min. The reaction was considered to be complete when the curve leveled off to a baseline. The cured sample was left in DSC cell and cooled to room temperature. To determine the glass transition temperature (T_g) of reacted product, the cured sample was scanned again to 623K at 10K/min. The intermediate point of the heat flow step of the second diagram was defined as DSC T_g. A set of three specimens was tested for each material.

Thermal diffusivity (δ, mm^2/s) at room temperature was measured on square plate samples ($10\times10\times1mm^3$) by laser flash method (nanoflash LFA 447 system, NETZSCH Instruments Japan Co., Ltd., a total of 5 shots were taken per sample set), specific heat (C, J/gK) at room temperature was measured on disk samples (6mm diameter, 1mm thickness) by DSC (NETZSCH DSC 204 F1 system, NETZSCH Instruments Japan Co., Ltd.), and bulk density (ρ, g/cm^3) of specimen was measured by water displacement. For each measurement, three samples were tested five times. After that, thermal conductivity (λ, W/mK) was calculated by using the equation: $\lambda=\delta\times C\times\rho$.

Thermal degradation behavior was characterized by TGA (TG-DTA200se/h/24/1 system, NETZSCH Instruments Japan Co., Ltd.) at a scan rate of 10 K/min to 1023K in N_2. A set of three specimens was tested for each material. Specimens were pre-dried in air at 373K for 12h to remove absorbed water.

Coefficient of thermal expansion (CTE) was tested on square plate samples ($25\times5\times1mm^3$) by SII TMA/SS7100 (Hitachi High-Tech Science Co., Japan, tensile mode with a 5mN load) at a heating rate of 5 K/min in N_2 atmosphere. The CTE values were determined from the second run of 303~443K profiles. A set of three specimens was tested for each material.

Wide angle X-ray diffractometry (WXRD) (Rigaku RINT RAPID II) with CuKa radiation (k = 0.154 nm) at a generator voltage of 40kV and current of 30mA was used to examine the crystal structure of samples in a 0˚~50˚ range of diffraction angles. A set of three specimens was tested for each material.

3. Results and discussion

3.1 Morphology and characterization of MGO

Morphology and characterization of MGO greatly determine its contribution to the

performance improvement of polymer matrix. As shown in the TEM image (Fig.1 (a)), MGO sheets with area of a few thousand square nanometers spread on the top of copper grid, where they look like crumpled silk veil waves, rippling and entangling with each other. The most transparent and featureless zones are likely to be monolayer local regions. Normal-incidence selected-area electron diffraction (SED) pattern (Fig.1 (b)) shows a typical hexagonal symmetry expected for graphite/graphene, which allows to be labeled with Miller-Bravais (*hkl*) indices. Monolayer GO owns a similar hexagonal pattern to that of MGO, and the main difference is that for monolayer, {2110} spots appear to be less intense than {1100} spots, i.e. $I_{\{1100\}}/I_{\{2110\}}>1$, whereas for multi-layers, $I_{\{1100\}}/I_{\{2110\}}<1$, this identification allows monolayer GO differentiated from MGO by inspection of the intensity ratio $I_{\{1100\}}/I_{\{2100\}}$ [29]. To do this, we plotted a line section through the (1-210)-(0-110)-(-1010)-(-2110) axis for the pattern in Fig.1 (b), it is noticeable that the inner peaks, (0-110) and (-1010), are more intense relative to the outer ones, (1-210) and (-2110), indicating that the tested multi-layer sample displays a ratio of $I_{\{1100\}}/I_{\{2110\}}>1$ in diffraction pattern and thus suggesting that some MGO were exfoliated into individual sheets or local region part of single monolayer exists and protrudes out of the MGO sheet edge.

SED gave an unambiguous local identification of monolayer. Nevertheless, it is not a reliable method to estimate the proportion of multi-layers in as-received product by testing SED of several sheets since SED can provide monolayer-like pattern for the multi-layers as the beam is incident on a protruding monolayer; better qualitative evaluation method is to observe the product in FE-SEM image [29]. The dimension of MGO sheets in Fig.1(c) is found from submicron to several micrometers, and the inserted image presents ~14.3 nm in thickness, indicating that many MGO sheets

utilized in this work are composed of ~29 stacked single-layer sheets since the average thickness of individually exfoliated GO sheet is ~0.486nm [30]. Furthermore, FTIR spectrum of MGO in Fig. 1(d) shows the presence of -OH and C=O groups [16, 17] which facilitate the chemical interactions of MGO sheets with the epoxy matrix, thus, the as-received MGO product are confirmed to have desirable functional groups.

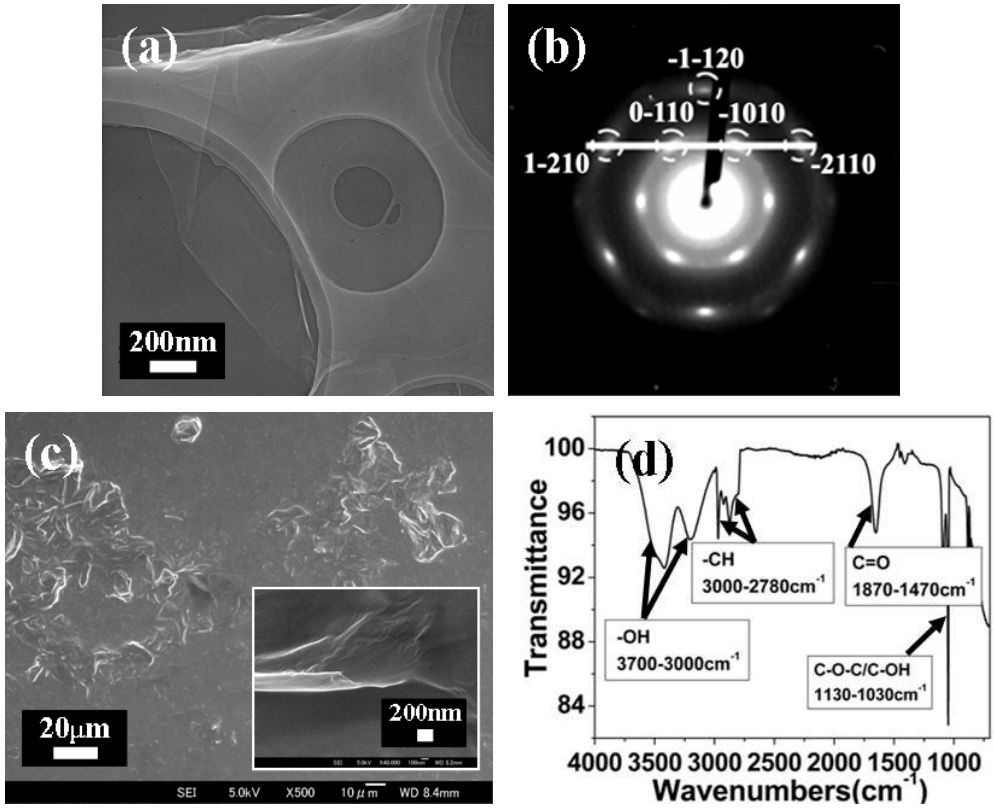

Fig.1 Evidence of MGO and monolayer local region. (a) TEM micrograph of as-received MGO sheets, (b) SED pattern of MGO sheets in (a), and (c) FE-SEM micrographs of MGO sheets ×500 (insert: ×40k). FTIR spectrum of MGO sheets (d) (inserts: explanatory notes for functional groups)

3.2 Identifying the optimal MGO content by a facile three-step strategy

(i) Observing the "unusual" effect of MGO content on the initial curing stage

DSC curves of neat epoxy and 1wt%MGO/epoxy system at different heating rates are shown in Fig.2 (a), and shift of exothermic peaks to higher temperature zone is observed in the presence of 1wt%MGO. To make an overall comparison, DSC curves at 10K/min heating rate of all the systems are presented in Fig.2 (b), it is clear that MGO inhibits the initial curing stage (reflected by increased exothermic peak temperature T_p tabulated in Table 1) at lower contents (0.5, 1wt %), then the inhibition effect is markedly abated at the 2wt%MGO before a further hindrance at 3wt%MGO. The "unusual" accelerating effect of 2wt%MGO on initial curing stage is partially due to the -OH groups of MGO sheets [30-32] since the matrix employed in this work was DGEBA/EMI-2,4 system, curing mechanism of which involves that O^-/OH initiates the etherification reaction during which epoxy monomers crosslink into network [33], however, such "unusual" catalytic effect can be primarily ascribed to the formation of conductive MGO percolating chains with enough MGO sheets present, which energize the surrounding epoxy molecules with unprecedented reactivity.

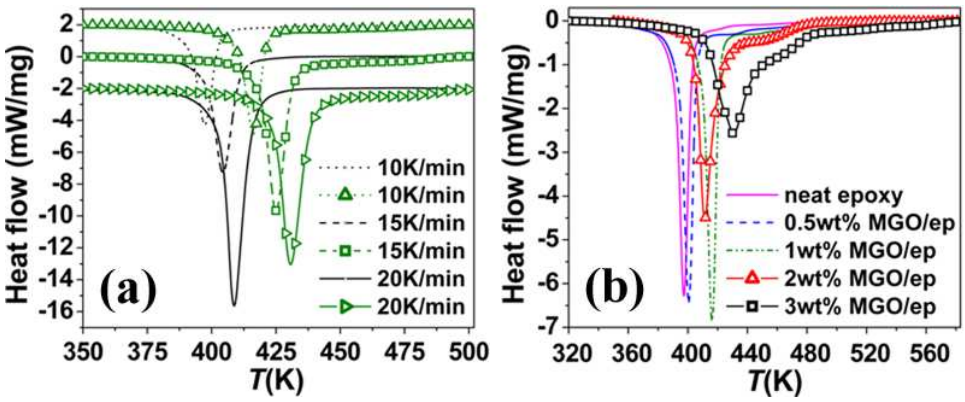

Fig.2 Dynamic DSC curves of (a) neat epoxy (line) and 1wt%MGO/epoxy system (line+symbols) at different heating rates, (b) all the systems at 10K/min heating rate.

Table 1 DSC-determined T_ps and total heats of reaction (ΔHs) at 10K/min heating rate; FTIR-determined α_{IR}s

Cured system	T_p(K)	ΔH(J/g)	α_{IR}
neat epoxy	398.28±0.20	495.2±1.2	0.92±0.01
0.5wt%MGO/epoxy	400.61±0.10	512.1±2.5	0.92±0.01
1wt%MGO/epoxy	416.27±0.15	582.2±2.7	0.94±0.01
2wt%MGO/epoxy	411.27±0.13	544.2±2.9	0.99±0.01
3wt%MGO/epoxy	430.60±0.07	656.3±1.5	0.97±0.01

(ii) Analyzing the "unusual" effect of MGO content on the later curing stage

A comparison of reaction extent (α) vs. T of all the systems is presented in Fig.3 (total area S of the exothermal peak, i.e. region between the exotherm and the baseline, is in direct proportion to the total heat of reaction ΔH, then α at any temperature T is: $\alpha=\Delta H_T/\Delta H=S_T/S$ ($0\leq\alpha\leq1$) [33]). It is noticed that besides the "unusual" accelerating effect of 2wt%MGO on the initial curing stage, there is a persistently prohibited curing at the later stage with increasing MGO content but no "unusual" phenomenon.

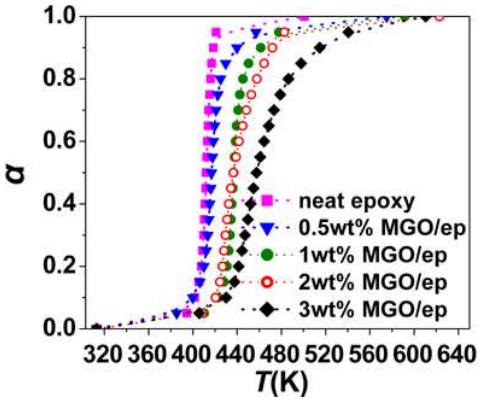

Fig.3 Reaction extent α vs. T at 25K/min heating rate. Lines are given only for showing the tendency.

To have an in-depth analysis, an effective method is employed herein, specifically,

α vs. T at different heating rates of all the systems investigated is presented in Fig.4(a), for each formulation all the curves have the same functional form, only shift a distance along the temperature axis, and should be superposable by simply shifting each curve along the temperature axis relative to a curve at an arbitrary reference heating rate by a shift factor, $\varphi(\beta)= T_{ref} - T_{\beta}$, where β is the heating rate [33].

Fig.4 (b) shows the superposed curves of α *vs.* T for all the systems taking the curve of 25K/min heating rate as the master curve. Master curve represents the progression of the reaction as a material is cured at a reference heating rate.

The phenomenological reaction rate, $d\alpha/dt$, has a general expression [33]:

$$d\alpha/dt = Ae^{-E/RT}f(\alpha) \quad (1)$$

where A is the frequency factor, E is the activation energy, $f(\alpha)$ is a function of reaction extent α, R is the gas constant and T is the absolute temperature at time t.

let $T = \beta t$, then $d\alpha/dT$ can be expressed as:

$$d\alpha/dT = Ae^{-E/RT}f(\alpha)/\beta$$

$$\ln(d\alpha/dT)-\ln[Af(\alpha)] = -E/RT-\ln\beta \quad (2)$$

As far as some arbitrary reaction extent α is concerned, the values of $\ln[Af(\alpha)]$ at different heating rates are equal while the values of $d\alpha/dT_{\beta}$, tangent slope of the point corresponding to α in the curves at different heating rates, are not always equal to that of reference curve i.e. $d\alpha/dT_{ref}$. Previous work [33] demonstrated that if the reaction is kinetically controlled, $d\alpha/dT_{\beta} > d\alpha/dT_{ref}$ as taking the curve of maximum heating rate as the master curve, that is to say, the curves of α *vs.* T should branch off from the master curve, and the shift factor $\varphi(\beta)= T_{ref} - T_{\beta}$ will increase as α increases.

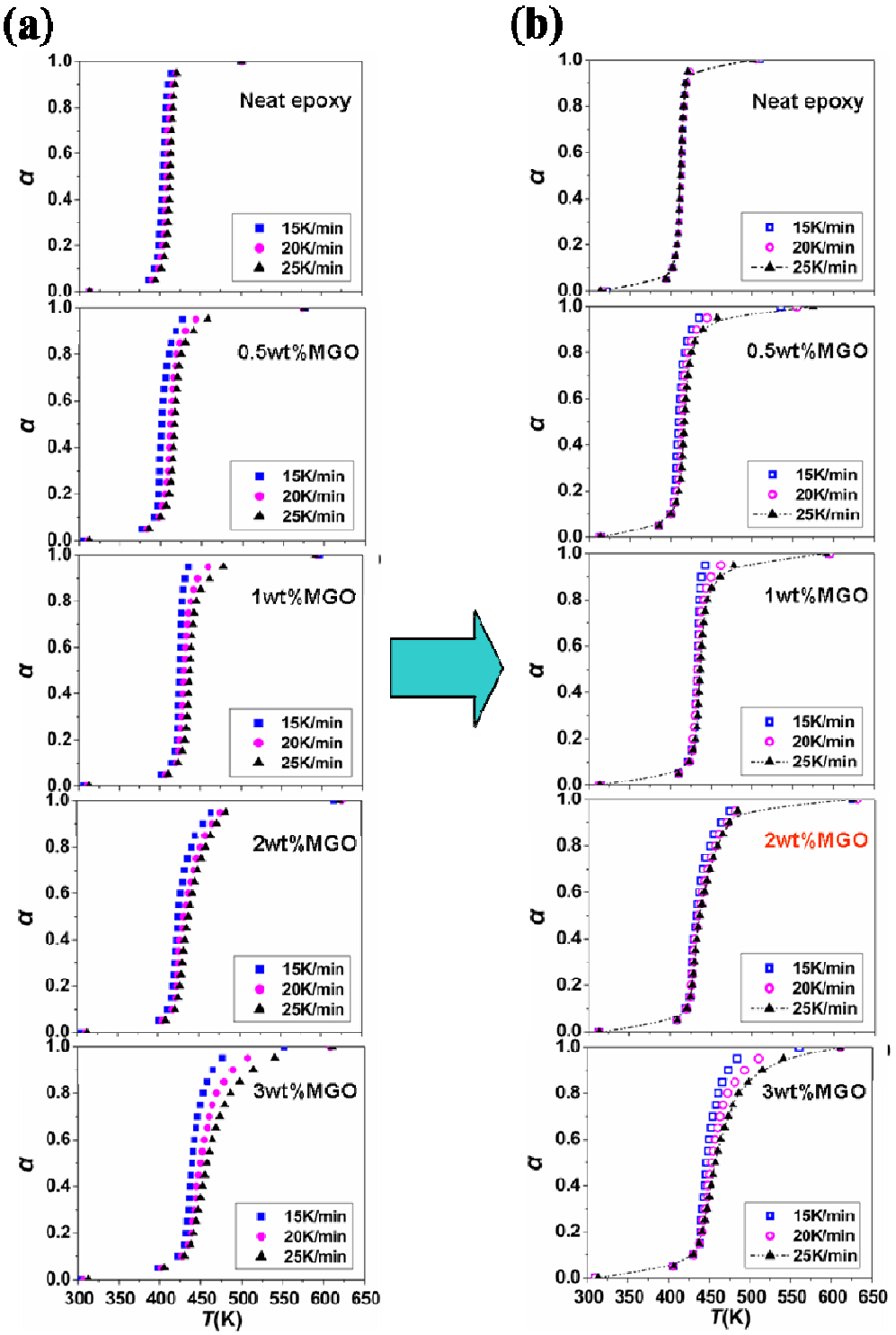

Fig.4 (a) Reaction extent α vs. T and (b) superposed curves of α vs. T of neat epoxy and MGO/epoxy systems. Dotted lines are given only for showing the tendency.

During the curing, system undergoes gelation (liquid-to-rubber) and vitrification (rubber-to-glass) transitions. As T_g increases over the curing temperature T_c, system vitrifies, reaction becomes diffusion controlled and the values of $d\alpha/dT_\beta$ decrease, i.e., curves of α vs. T do not shift enough from the master curve, although we do not know the exact degree the curves should shift from the master curve, a qualitative comparison can be made [33]. As far as the curves in Fig.4 (b) are concerned, vitrification degree follows a sequence of 3wt%MGO<1wt%MGO<0.5wt%MGO<2wt%MGO<neat epoxy, highlighting an "unusual" promotion effect of 2wt%MGO on vitrification.

The "unusual" promoted vitrification was also supported by the "unusual" increase effect of 2wt%MGO on T_g as shown in Fig.5.

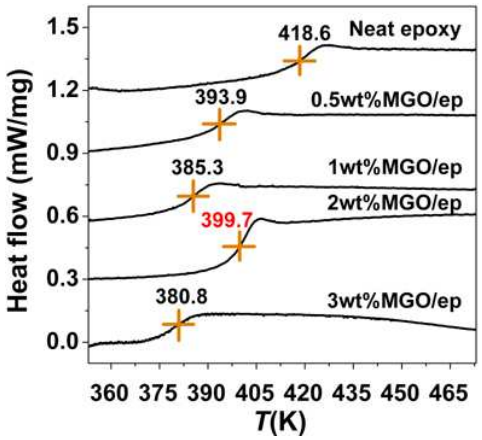

Fig.5 Dynamic DSC curves of all the cured systems for determining T_g

T_g decreases with the increasing MGO content (0.5, 1, 3wt %), which can be due to an antagonistic competition of two effects. So far the increased T_g for epoxy resins in the presence of small amount of GO (≤0.5wt%GO [34, 35]) are mainly attributed to the reaction of epoxide with functional groups of GO [36], herein, the chemical bonding in MGO/epoxy interface as well as the physical hindrance of MGO hampers the epoxy

motion, contributing to an enhancing effect on T_g since T_g increases with the increasing restriction imposed by crosslinking on the epoxy motion [33]. On the other hand, massive MGO sheets disrupt the crosslinking of epoxy matrix [36], -OH concentration gradient originated from the -OH groups of MGO sheets exerts the driving force on the diffusion of unreacted epoxy for epoxy-MGO reaction, what's more, the diffusion is facilitated by the extra free volume derived from the tremendous MGO/epoxy interface [33], as a result, a final lowering effect of MGO (0.5, 1, 3wt %) on T_g occurs. Inhibited vitrification keeps the cure reaction under long-term kinetic control until higher temperature zone, resulting in increased heat of reaction ΔH (see Table1), e.g. the lowest T_g whereas the highest ΔH of 3wt%MGO/epoxy composite.

More importantly, the "unusual" increase effect of 2wt%MGO on T_g confirms the existence of 2wt%MGO chains percolating throughout the matrix. Steep temperature gradient caused by these heat-flow preferred percolating chains intensively promotes the epoxy-MGO reaction as well as epoxy crosslinking, leading to a strong MGO/epoxy interfacial bonding (will be discussed below) and the highest epoxy curing degree α_{IR} (see Table1), thus producing a predominant restriction on epoxy motion and the "unusual" increase effect on T_g.

(iii) Observing the "unusual" double-peak pattern of curing curves

It is interesting to note in Fig.2 (b) that the exothermal peak first obviously splits into two peaks at the 2wt%MGO content. To analyze this "unusual" double-peak pattern, epoxy-MGO reaction should be highly valued based on the two facts that: (1) large amount of epoxy molecules are isolated by MGO sheets, (2) -OH groups on/within MGO sheet also initiate the reaction of etherification (evidenced by the higher ΔH of MGO/epoxy composites than that of neat epoxy standardized by the same α_{IR} e.g.

ΔH(2wt%MGO/epoxy composite, 544.2 J/g) > 0.99/0.92 ΔH(pure epoxy, 495.2 J/g)), as a result, hydrogen bonds form at the MGO/epoxy interface (confirmed by the downshift of peaks of -OH group to the lower wavenumber (see Fig.6 (a)) since the formation of hydrogen bonding in GO/polymer composites can be examined by the vibration peak position of -OH group [37]).

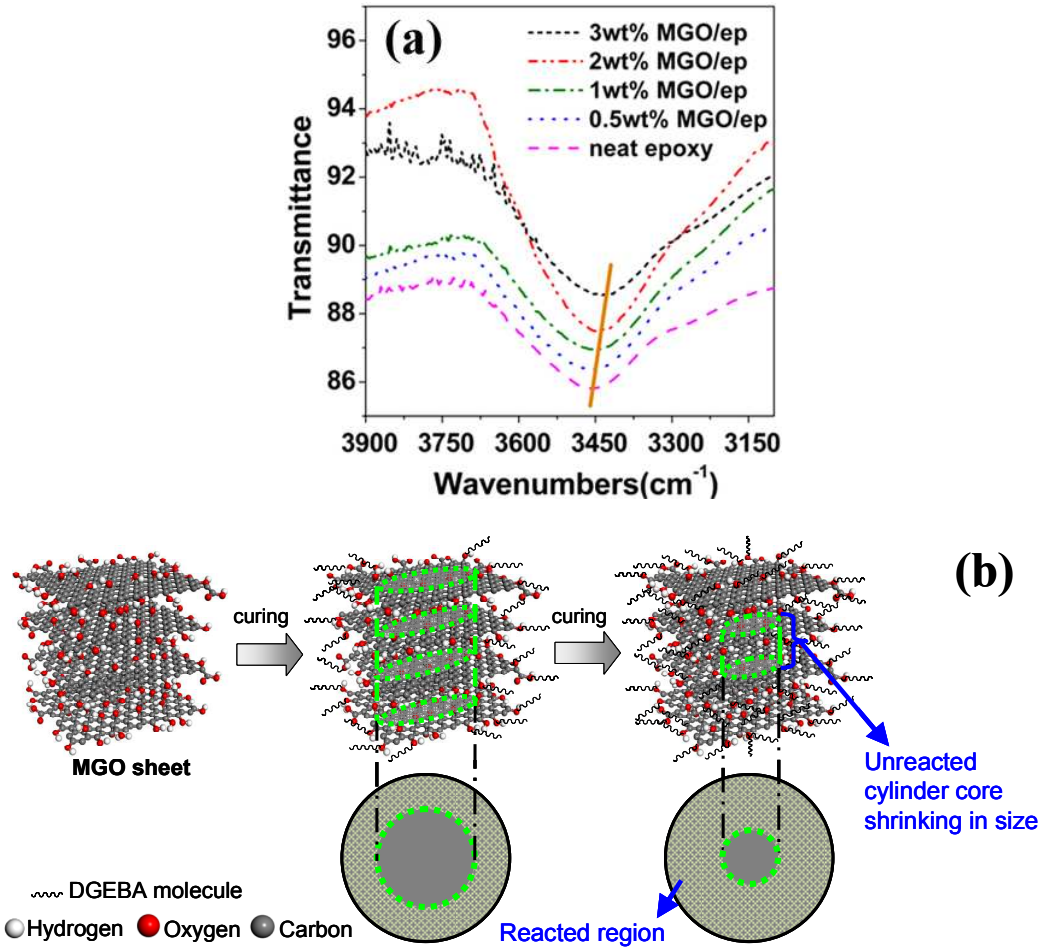

Fig.6 (a) FTIR spectra of all the cured systems, showing the vibration of -OH groups at wavenumbers 3100-3700cm^{-1}, (b) illustration of modified Shrinking Core Model.

Epoxy-MGO reaction can be studied using Shrinking Core Model, the best simple representation for majority of reacting fluid-particle systems [38-40]. Here, the original

sphere-shell model was modified with a cylinder-shell model customized for the special layered-structure of MGO sheet (see Fig.6 (b). Epoxy-MGO reaction occurs first at the outer skin of MGO sheet, and then the zone of reaction moves into intersheet and leaves behind reacted cylindrical zone, i.e. three steps occur in succession: (1) diffusion of DGEBA molecule through the liquid film surrounding the MGO sheet to the surface of MGO sheet, (2) penetration into the intersheet space of MGO and diffusion of DGEBA molecule through the reacted region to the surface of unreacted cylinder core part, and (3) reaction of DGEBA molecule with the unreacted cylinder core at the interface of the reacted region and unreacted core region. The resistance of different steps usually varies greatly, in such case, step with the highest resistance is rate-controlling, the progressive reaction of epoxy-MGO system is chemical reaction, reacted region diffusion, and liquid film diffusion in turn control.

The whole reaction, including the epoxy crosslinking and the epoxy-MGO reaction, can therefore be simply divided into two stages i.e. chemical reaction-controlling and diffusion-controlling stages, reflected as the double-peak pattern [41].

The amount of curing heat released during the two stages determines the peak-area proportion. As MGO contents are low, the second peak tends to overlap with the first one (0.5wt %) or is only a negligible small peak (1wt %) as shown in Fig.2 (b). However, as 2wt%MGO is added, an obvious double-peak pattern starts to appear, indicating an unprecedented amount of curing heat released at the diffusion-controlling stage, such a qualitative change reconfirms the existence of MGO percolating chains with 2wt%MGO sheets present, which unprecedentedly promote the diffusion of epoxy for cure reaction.

Further increasing the MGO content e.g. 3wt% leads to more reactions inhibited

until the diffusion-controlling stage, as a result, the second peak gets stronger with the first peak diminished as shown in Fig. 2(b). However, a sharply increased viscosity had already been noted as preparing the 2wt%MGO/epoxy composite mixture with MGO agglomerates impossible to be cleared in the case of higher MGO content. Therefore, among the formulations in this work, 2wt%MGO is finally identified as the critical content owning the optimal strengthening effect on the thermal conductivity of epoxy, considering the unavoidable MGO agglomerates in 3wt%MGO/epoxy composite.

Furthermore, 2wt%MGO also led to the highest T_g which acts as a key role in determining the structural thermal stability and the CTE value, therefore, 2wt%MGO is identified as the critical content among the formulations here for epoxy composite with the optimal thermal properties.

Apparently, further research is needed to identify the percolating threshold within 1~2wt%MGO or more precisely identify the optimal MGO content by extending the formulations such as 2.1, 2.2, 2.3, … , 2.8, 2.9wt% MGO, and they are beyond the scope of this study.

3.3 Verifying the optimal MGO content by thermal properties

To verify the optimal MGO content, the general procedure as afore-described in Introduction part was performed, i.e. the cured samples were processed (cut, grinded, and finely polished) followed by property testing with the results (thermal conductivity, thermal degradation behaviors and CTE) presented in Figs.7-9. It is common to consider the half-weight-loss temperature (T_{half}) as the indicator for the beginning of the structural decomposition, therefore T_{half}, as well as char yield (1023K), obtained from Fig. 8 is also summarized in Table 2.

The critical MGO content for the optimal thermal conductivity was verified by two

facts: (1) as shown in Fig.7, thermal conductivity rises slowly at low MGO contents (0.5, 1wt %), then exhibits a sharp rise at the 2wt% MGO, reaching a maximum (2.03 times that of the epoxy); (2) at the initial and the later thermal degradation stages (see the insets in Fig.8), accelerated thermal degradation are noticed with the 2wt%MGO, evidencing the existence of thermally conductive 2wt%MGO percolating chains which markedly promote the thermal degradation, especially after structural decomposition commences and consequently result in a relative lower char yield of 2wt%MGO/epoxy composite than that of 1wt%MGO/epoxy composite (see Table 2).

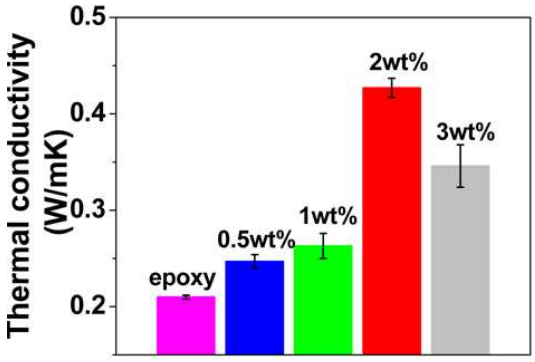

Fig.7 Thermal conductivities of neat epoxy and MGO/epoxy composites

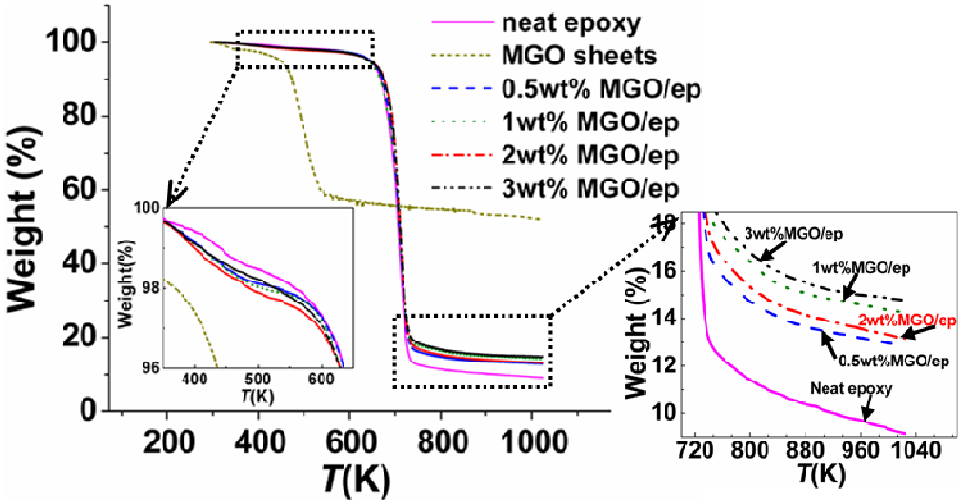

Fig.8 TGA curves of neat epoxy, MGO sheets and MGO/epoxy composites (inserts: enlargement of the boxed regions)

Table 2 T_{half}s and char yields (1023K) of neat epoxy, MGO sheets and MGO/epoxy composites

Sample	T_{half} (K)	Char yield (%)
neat epoxy	706.8±0.1	9.1±0.1
MGO sheets	/	52.2±0.2
0.5wt%MGO/epoxy composite	708.8±0.1	12.9±0.1
1wt%MGO/epoxy composite	708.4±0.1	14.2±0.1
2wt%MGO/ epoxy composite	711.8±0.2	13.2±0.1
3wt%MGO/ epoxy composite	710.4±0.1	14.8±0.1

The critical MGO content for the optimal structural thermal stability is proved, based on the fact that the maximum T_{half} is achieved at the 2wt%MGO (see Table 2), which can be due to the highest structure-determined T_g of 2wt%MGO/epoxy composite among all the formulations investigated [42, 43] as well as the effective barrier-effect of 2wt% MGO which retards the decomposition of epoxy by the even dispersion of MGO sheets (will be discussed below) [30].

Also, the critical MGO content for the optimal CTE is supported by the remarkable reduction in CTE, 23% reduction in CTE, at the 2wt% MGO content shown in Fig.9. CTE of MGO/epoxy composites originates in three parts: MGO, epoxy matrix and MGO/epoxy interface. Besides the relatively rigid of MGO sheets, the reduction in CTE of 2wt%MGO/epoxy composite can be attributed to the strongly enhanced MGO/epoxy interface by the intensively promoted epoxy-MGO reaction with heat-flow preferred 2wt%MGO percolating chains. Normally, neat epoxy is featureless smooth area with a typical brittle fracture process, whereas improved surface roughness (see the insert) is accompanied by a creation of plastic deformation of matrix, confirming the existence of strongly bonded MGO/epoxy interface.

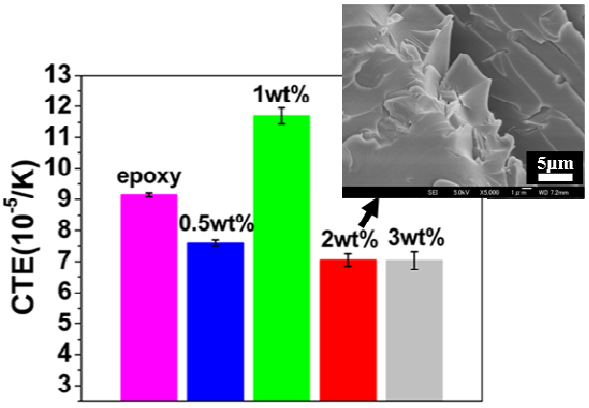

Fig.9 CTE values of neat epoxy and MGO/epoxy composites (insert: FE-SEM image of the fracture surface of 2wt% MGO/epoxy composite)

Additionally, as expected, further increase of thermal properties failed to realize at 3wt%MGO, and the supposed MGO agglomerates which significantly reduce the effectiveness of MGO for forming conductive network are also confirmed by WXRD, FE-SEM and TEM results (see Fig.10): (i) WXRD pattern of graphite particles exhibits a sharp characteristic peak centered at 2θ=26.6° and a small characteristic peak centered at 2θ=43.3° (see Fig.10 (a)), which are assigned to the diffraction of (002) and (100) planes of well-ordered graphenes, respectively [36]. The as-received MGO sheets keep the small one and the sharp characteristic peak disappears, which is associated with a high disorder in the direction perpendicular to MGO layers [36] (The sharp peak at 2θ=26.6° in graphite usually shifts to 14.1°-14.9° in graphite oxide, however, the peak would disappear as graphite oxide exfoliates into singer sheets [44]. The small peak centered at 2θ=43.3° usually remains in graphite oxide [36] or MGO sheets [45]). Notably, after dispersed into epoxy, WXRD patterns of 0.5, 1, 2wt%MGO/epoxy composites only show a broad diffraction peak originated from amorphous epoxy centered at 2θ=18.5°; the small peak disappears, which indicates a complete disorder in

the direction perpendicular to GO layers, clearly demonstrating the highly exfoliated level of MGO in matrix as MGO content is up to 2wt% [36, 44, 46, 47]. Subsequently a small diffraction peak of MGO appears, verifying that MGO restacks in matrix at 3wt% content; (ii) it can be observed in FE-SEM images (Fig.10 (b)) that numerous tortuous and fine river-like structures with hackles and ribbons exist on the fracture surface, suggesting the highly dispersed state of 0.5, 1, 2wt%MGO in matrix [30, 34], comparatively, more bigger tortuous and river-like structures especially the agglomerates circled in Fig.10 (b) clearly confirms that the restacks of MGO present in 3wt%MGO/epoxy composite; (iii) TEM images (Fig.10 (c)) further reconfirm the highly dispersed state of 0.5, 1, 2wt%MGO in matrix, while large MGO agglomerate emerges in 3wt%MGO/epoxy composite.

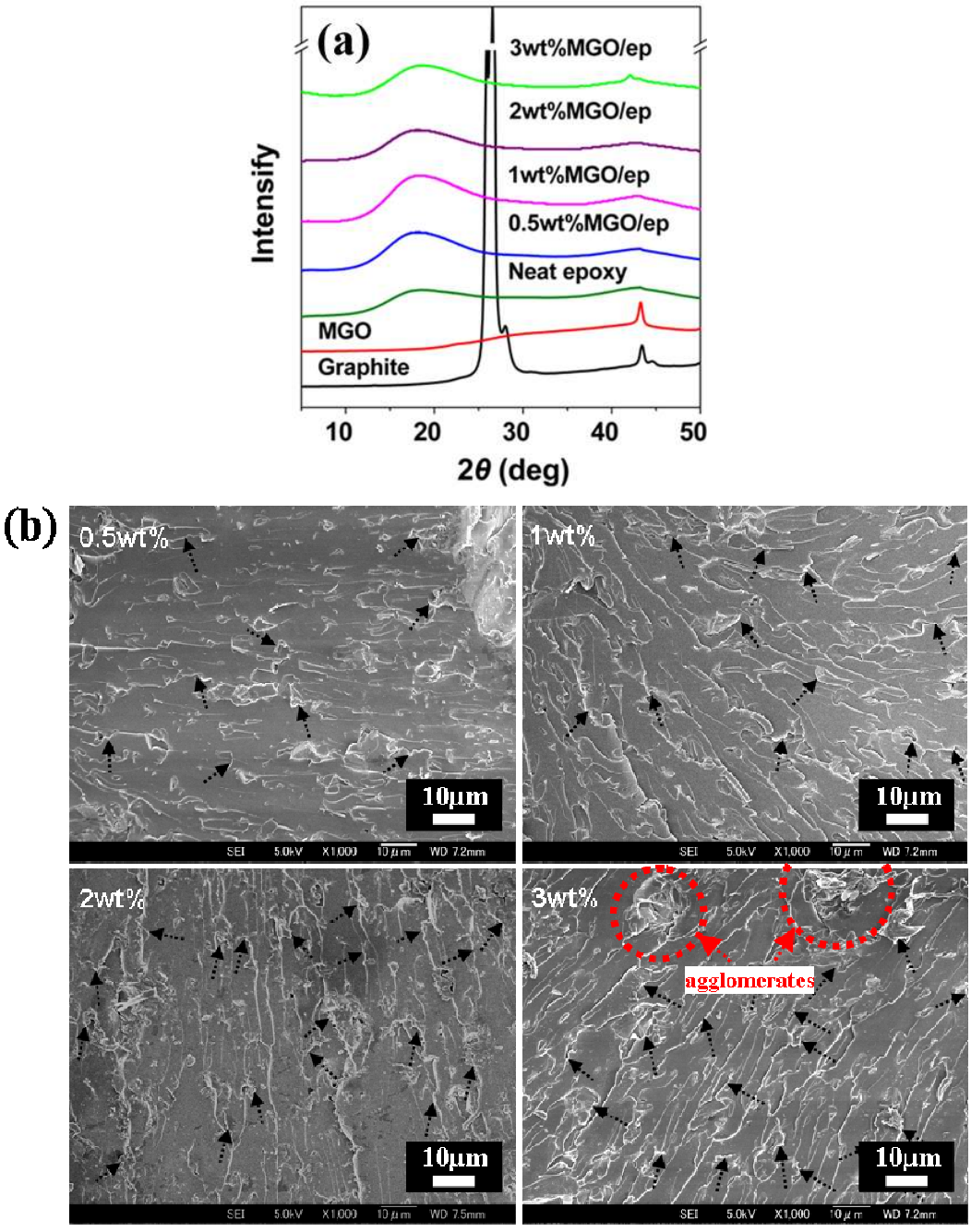

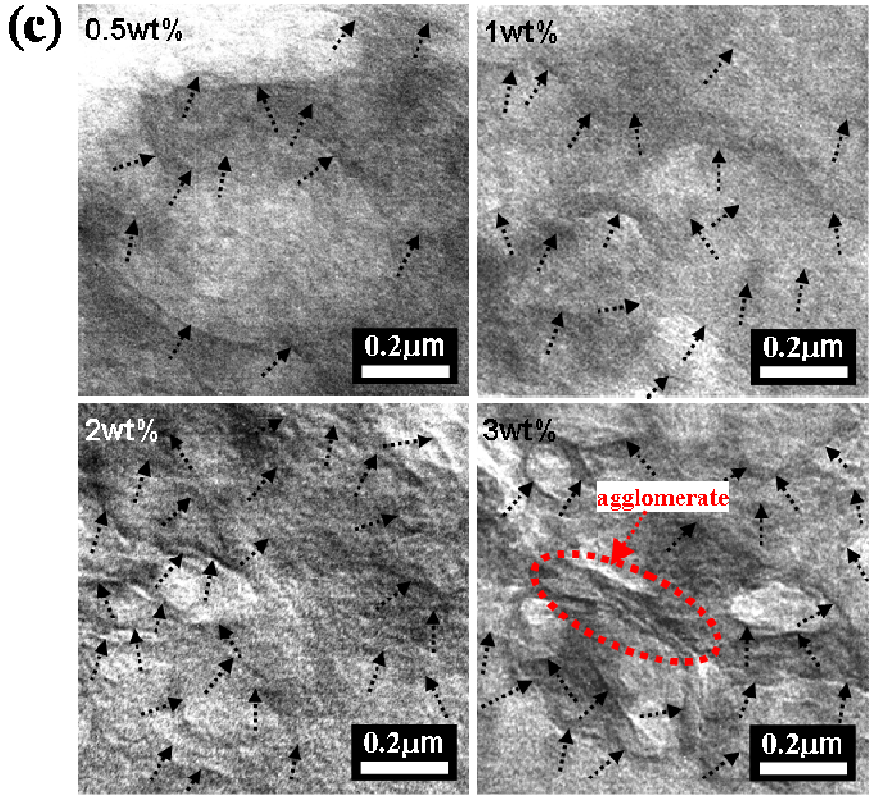

Fig.10 (a) WXRD patterns of graphite, MGO, neat epoxy, and MGO/epoxy composites, (b) FE-SEM images of the fracture surface and (c) TEM images of MGO/epoxy composites. Dotted arrows show MGO, circles and ellipse show MGO agglomerates.

4. Conclusions

A facile strategy was demonstrated for the rapid identification of the critical MGO content among formulations for epoxy composite with the optimal thermal properties. The strategy proceeds without complicated and time-consuming works e.g. processing samples (cutting, grinding, finely polishing, etc) and testing various properties, which is required in general procedure. Operation is simple and requires only the monitoring of "unusual" curing phenomena. It opens up a simple avenue to determine the optimal MGO content thus quickening the development of thermally conductive MGO/polymer

composites, and it can be readily adapted by academic researches and industry applications for different kinds of conductive polymer composites.

Acknowledgements

The authors are grateful for the financial support of National Natural Science Foundation of China (No.51203074), Fundamental Research Funds for the Central Universities (No. NUST 2011YBXM163), Jiangsu Overseas Research & Training Program for University Prominent Young & Middle-aged Teachers and Presidents, and Special Foundation for 'first-grade Zijin's Star' of "Excellence initiative" Project of Nanjing University of Science and Technology (No.AB41339).

References

[1] K. K. Sadasivuni, D. Ponnamma, S. Thomas and Y.Grohens, *Prog. Polym. Sci.*, 2014, **39**, 707.

[2] X. Sun, H. Sun, H. Li and H. Peng, *Adv. Mater.*, 2014, **25**, 5153.

[3] C. J. Shearer, A. Cherevan and D. Eder, *Adv. Mater.*, 2014, **26**, 2295.

[4] X. Mao, G. C. Rutledge and T. A. Hatton, *Nano Today*, 2014, **9**, 405.

[5] K. Suganuma, *Introduction to printed electronics*, Springer Science+Business Media, New York, USA, 2014.

[6] Q. Zheng, Z. Li, J. Yang and J-K. Kim, *Prog. Mater. Sci.*, 2014, **64**, 200.

[7] H. Deng, L. Lin, M. Ji, S. Zhang, M. Yang and Q. Fu, *Prog. Polym. Sci.*, 2014, **39**, 627.

[8] Q. Li, Y. Guo, W. Li, S. Qiu, C. Zhu, X. Wei, M. Chen, C. Liu, S. Liao, Y. Gong, A. K. Mishra and L. Liu, *Chem. Mater.*, 2014, **26**, 4459.

[9] C-Y. Chang, S-P. Ju, J-W. Chang, S-C. Huang and H-W. Yang, *RSC. Adv*., 2014, **4**, 26074.

[10] J. Syurik, N. Alyabyeva, A. Alekseev and O. A. Ageev, *Comp. Sci. Technol*., 2014, **95**, 38.

[11] A. Noël, J. Faucheu, J-M. Chenal, J-P. Viricelle and E. Bourgeat-Lami, *Polymer*, 2014, **55**, 5140.

[12] P. Ding, S. Su, N. Song, S. Tang, Y. Liu and L. Shi, *Carbon*, 2014, **66**, 576.

[13] N-W. Pu, Y-Y. Peng, P-C. Wang, C-Y. Chen, J-N. Shi, Y-M. Liu, M-D. Ger and C-L. Chang, *Carbon*, 2014, **67**, 449.

[14] W. Park, J. Hu, L. A. Jauregui, X. Ruan and Y. P. Chen, *Appl. Phy. Lett*., 2014, **104**, 11301.

[15] S. Araby, Q. Meng, L. Zhang, H. Kang, P. Majewski, Y. Tang and J. Ma, *Polymer*, 2014, **55**, 201.

[16]M. Zeng, J. Wang, R. Li, J. Liu, W. Chen, Q. Xu and Y.Gu, *Polymer*, 2013, **54**, 3107.

[17] A. Allahbakhsh, S. Mazinani, M. R. Kalaee and F. Sharif, *Thermochim. Acta*., 2013, **563**, 22.

[18] X. Wang, J. Jin and M. Song, *Eur. Polym. J*., 2012, **48**, 1034.

[19] Z. Qiu and H. Wang, *Thermochim. Acta*., 2011, **527**, 40.

[20] S. L. Qiu, C. S. Wang, Y. T. Wang, C. G. Liu, X. Y. Chen and H. F. Xie, *Express. Polym. Lett*., 2011, **5**, 809.

[21] S. H. Ryu, J. H. Sin and A. M. Shanmugharaj, *Eur. Polym. J*., 2014, **52**, 88.

[22] W. Liu, K. L. Koh, J. Lu, L.Yang, S. Phua, J. Kong, Z. Chen and X. Lu, *J. Mater. Chem*., 2012, **22**, 18395.

[23] X. Jing and Z. Qiu, *J. Nanosci. Nanotechno*., 2012, **12**, 7314.

[24] X. Jing and Z.Qiu, *Ind. Eng. Chem. Res*., 2012, **51**, 13686.

[25] M. Martin-Gallego, M. Hernández, V. Lorenzo, R.Verdejo, M. A. Lopez-Manchado and M. Sangermano, *Polymer*, 2012, **53**, 1831.

[26] M. Martin-Gallego, R. Verdejo, M. A. Lopez-Manchado and M. Sangermano, *Polymer*, 2011, **52**, 4664.

[27] K. Deshmukh and G. M. Joshi, *RSC. Adv*., 2014, **4**, 37954.

[28] I. Zaman, T. T. Phan, H-C. Kuan, Q. Meng, L. T. B. La, L. Luong, O. Youssf and J. Ma, *Polymer*, 2011, **52**, 1603.

[29] Y. Hernandez, V. Nicolosi, M. Lotya, F. M. Blighe, Z. Sun, S. De, I. T. McGovern, B. Holland, M. Byrne, Y. K. Gun'Ko, J. J. Boland, P. Niraj, G. Duesberg, S. Krishnamurthy, R. Goodhue, J. Hutchison, V. Scardaci, A. C. Ferrari and J. N. Coleman, *Nat. Nanotechnol*., 2008, **3**, 563.

[30] Y-J. Wan, L-C. Tang, L-X. Gong, D. Yan, Y-B. Li, L-B. Wu, J-X. Jiang and G-Q. Lai, *Carbon*, 2014, **69**, 467.

[31] B. Shen, W. Zhai, M. Tao, D. Lu and W. Zheng, *Comp. Sci. Technol*., 2013, **77**, 87.

[32] V. Patil, R. V. Dennis, T. K. Rout, S. Banerjee and G. D. Yadav, *RSC Adv*., 2014, **4**, 49264.

[33] T. Zhou, M. Gu, Y. Jin and J. Wang, *Polymer*, 2005, **46**, 6216.

[34] L-C. Tang, Y-J. Wan, D. Yan, Y-B. Pei, L. Zhao, Y-B. Li, L-B. Wu, J-X. Jiang and G-Q. Lai, *Carbon*, 2013, **60**, 16.

[35] X-J. Shen, X-Q. Pei, S-Y. Fu and K. Friedrich, *Polymer*, 2013, **54**, 1234.

[36] M. Mauro, M. R. Acocella, C. E. Corcione, A. Maffezzoli and G. Guerra, *Polymer*, 2014, **55**, 5612.

[37] C. L. Bao, Y. Q. Guo, L. Song and Y. Hu, *J. Mater. Chem.*, 2011, **21**, 13942.

[38] T. Zhou, M. Gu, Y. Jin and J. Wang, *J. Polym. Sci. Pol. Chem.*, 2006, **44**, 371.

[39] T. Tilman, K. Markus, G. Friedrich and J. M. E. Bastian, *Chem. Eng. Sci.*, 2012, **69**, 492.

[40] B-H. Shi, S-S. Fan and X. Lou, *Chem. Eng. Sci.*, 2014, **109**, 315.

[41] J. Wu, W. Xing, G. Huang, H. Li, M. Tang, S. Wu and Y. Liu, *Polymer*, 2013, **54**, 3314.

[42] S. Stankovich, D. A. Dikin, G. H. B. Dommett, K. M. Kohlhaas, E. J. Zimney, E. A. Stach, R. D. Piner, S. T. Nguyen and R. S. Ruoff, *Nature*, 2006, **442**, 282.

[43] M. A. Rafiee, J. Rafiee, I. Srivastava, Z. Wang, H. Song, Z-Z. Yu and N. Koratkar, *Small*, 2010, **6**, 179.

[44] H. Kim, A. A. Abdala and C. W. Macosko, *Macromolecules*, 2010, **43**, 6515.

[45] Y. F. Huang and C. W. Lin, *Polymer*, 2012, **53**, 2574.

[46] L-Z. Guan, Y-J. Wan, L-X. Gong, D. Yan, L-C. Tang, L-B. Wu, J-X. Jiang and G-Q. Lai, *J. Mater. Chem. A.*, 2014, **2**, 15058.

[47] Y-J. Wan, L-X. Gong, L-C. Tang, L-B. Wu and J-X. Jiang, *Compos. Part A-Appl. S.*, 2014, **64**, 79.

Facile identification of the critical content of multi-layer graphene oxide for epoxy composite with the optimal thermal properties

GRAPHICAL ABSTRACT

Description

A strategy to rapidly identify the critical content of multi-layer graphene oxide for epoxy composite with the optimal thermal properties.

Graphical